analytical chemistry

Article

pubs.acs.org/ac

Novel Model of Negative Secondary Ion Formation and Its Use To Refine the Electronegativity of Almost Fifty Elements

Klaus Wittmaack*

Helmholtz Zentrum München, Institute of Radiation Protection, 85758 Neuherberg, Germany

ABSTRACT: This study aimed to examine the recently proposed idea that the ionic contribution to atomic bonds is essential in determining the charge state of sputtered atoms. Use was made of negative secondary ion yields reported by Wilson for a large number of elements implanted in silicon and then sputter profiled by Cs bombardment. The derived normalized ion yields (or fractions) P vary by 6 orders of magnitude, but the expected exponential dependence on the electron affinity EA is evident only vaguely. Remarkably, a correlation of similar quality is observed if the data are presented as a function of the ionization potential IP. With IP being the dominant (if not sole) contributor to the electronegativity χ, one is led to assume that P depends on the sum χ + EA. About 72% of the "nonsaturated" ion yields are in accordance with a dependence of the form $P \propto \exp[(\chi + \mathrm{EA})/\varepsilon]$, with $\varepsilon \cong 0.2$ eV, provided the appropriate value of χ is selected from the electronegativity tables of Pauling (read in eV), Mulliken or Allen. However, each of the three sources contributes only about one-third to the favorable electronegativity data. This unsatisfactory situation initiated the idea to derive the "true" electronegativity χ_{SIMS} from the measured ion yields $P(\chi + \mathrm{EA})$, verified for 48 elements. Significant negative deviations of χ_{SIMS} from a smooth increase with increasing atomic number are evident for elements with special outer-shell electron configurations such as $(n-1)d^{g-1}ns^1$ or $(n-1)d^{10}ns^2np^1$. The results strongly support the new model of secondary ion formation and provide means for refining electronegativity data.

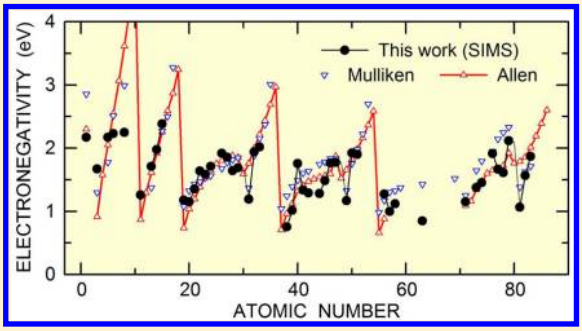

Secondary ion yields of different elements embedded in the same matrix are known to vary by more than 6 orders of magnitude, for positive[1−3] as well as for negative ions.[3−5] Previous attempts to rationalize available data were based on the idea that ion yields are determined by three parameters: (i) the work function of the sample, (ii) the velocity of the emitted atom, and (iii) its ionization potential IP (positive ions) or electron affinity EA (negative ions). However, as shown in a very detailed recent review,[6] the efficiency of secondary ion formation is not controlled by *global* electronic sample properties such as the work function. In fact, with cesium serving to enhance negative secondary ion formation, the yields were found to scale quantitatively with the availability of cesium at the ion-bombarded surface. The assumption that ion yields or the ion fractions in the flux of sputtered atoms are velocity dependent could be invalidated on the basis of a proper distinction between reliable and nonreliable experimental data.[6] Presenting ion fractions as a function of IP or EA one finds some general trends[6,7] yet with frequent deviations by more than 1 order of magnitude in either direction.

Here we examine the idea[6] that ion yields depend not only on the electronic properties of the sputtered atom but also on the *local* chemistry at the emission site which can be expected to also control the strength of the ionic contribution to interatomic bonding. This leads to the hypothesis that the (difference in) electronegativity χ of the atoms forming the bond is an important factor in determining ion yields. Quantitative evaluations suffer from the fact that a unique method for calculating χ does not exist. Hence it came as a surprise, in course of this study, that measured ion yields can serve to refine available electronegativity data.

EXPERIMENTAL SECTION

Data Basis: From Relative Sensitivity Factors to Normalized Ion Fractions. The data evaluated in this study were derived from the work of Wilson.[5] Samples were prepared by implanting a remarkably large variety of (impurity) elements in silicon substrates. Negative ion yields of the implanted species (dopants) and as well as of the substrate (matrix) atoms were determined using standard procedures of depth profiling by secondary ion mass spectrometry (SIMS). The measurements were performed using magnetic sector field instruments (Cameca IMS-3f or -4f).[6] The samples were bombarded with raster-scanned primary ion beams of 14.5 keV Cs^+ incident at an impact angle of about 25° to the surface normal. Details of instrument setting such as the chosen contrast aperture and the slit width on the exit side of the energy analyzer were not specified.

The measured (or known) quantities include the implantation fluence $\varphi_{i,j}$, the yields (count rates) $I_{i,j}$ due to the implanted isotopes j of element i, summed up over the whole implantation

Received: March 19, 2014
Accepted: May 13, 2014
Published: May 13, 2014

   dx.doi.org/10.1021/ac501006g | *Anal. Chem.* 2014, 86, 5962−5968

profile, $\sum I_{i,j}$, the stationary yields $I_{m,k}$ due to isotopes k of matrix element m, the respective isotopic abundance $\gamma_{m,k}$ and the depth interval Δz sputtered per frame (assuming the same data acquisition time per frame for dopant and matrix atoms). Using these numbers, the authors[4,5] defined a relative sensitivity factor $RSF_{i,m}$ as[6]

$$RSF_{i,m} = \frac{I_{m,k}/\gamma_{m,k}\Delta z}{\Sigma I_{i,j}/\phi_{i,j}} \quad (1)$$

The RSF values, quoted in units of atoms/cm^3, scale with the number density n_m of the reference target atoms. The correlation with the ionized fractions P_i and P_m of sputtered atoms i and m reads[6]

$$RSF_{i,m} = \frac{T_m \varsigma_m P_m}{T_i \varsigma_i P_i} n_m \quad (2)$$

where T_i and T_m denote the instrument transmission for the respective element and ς_i and ς_m the detection efficiencies. Note that $RSF_{i,m}$ is proportional to P_m/P_i, the *inverse* ratio of the ion fractions of impurity and matrix atoms. To simplify data evaluation, measured ion yields are normalized to the yields of those impurity species which feature high ion fractions in combination with small matrix effects.[8] In the case of negative SIMS, halogen ions serve the purpose reasonably well.[6,8] Identifying the reference species by subscript r, the impurity-to-reference ratio of ion fractions, the "normalized ion fraction" $P_{i,r}$ is written

$$P_{i,r} \equiv \frac{P_i}{P_r} = \frac{T_r \varsigma_r RSF_{r,m}}{T_i \varsigma_i RSF_{i,m}} \cong \frac{RSF_{r,m}}{RSF_{i,m}} \quad (3)$$

Given the fact that $T\varsigma$ values were not determined,[4,5] the RSF-data were converted using eq 3 under the assumption $T_r\varsigma_r/T_i\varsigma_i = 1$. The halogen ions F^-, Cl^-, Br^-, and I^- served as reference species; their RSF values[4,5] were found to be the same within a narrow margin, $(7.2 \pm 0.3) \times 10^{21}$ atoms/cm^3.

Normalized ion fractions thus derived are compiled in Figure 1. Experimentally determined electron affinities were taken from a comprehensive compilation,[9] supplemented by additional data[10−12] and an update.[13] The solid circles (open triangles) denote 55 (46) out of a total of 63 (51) RSF-data reported by Wilson[5] (Wilson and Novak[4]). The missing 8 (5) data are those for which experimentally determined electron affinities are not available or which are known to be metastable (Be).[14] Overall, the two sets of ion fractions show very good agreement, with four outliers exhibiting deviations by about a factor of 3 in one or the other direction and one extreme outlier (Eu, difference by a factor of 9). Owing to the broader data basis only the 1995 data[5] are examined here.

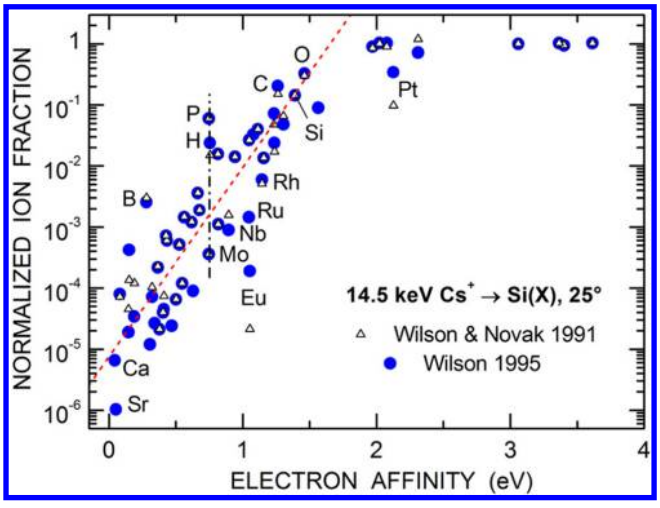

Figure 1. Negative ion fractions of elements implanted in silicon and subsequently sputter profiled by Cs bombardment. Raw data from refs 4 and 5. One typo in ref 5 was removed: the RSF of *K* should read 1.1 × 10^{26} cm^{-3}, as in ref 4 (R. G. Wilson, personal communication, 2013).

According to Figure 1, the normalized negative-ion fractions $P_{i,F}$ depend very strongly on the electron affinity of the sputtered element. In fact, in the range 0 < EA < 2 eV, $P_{i,F}$ increases, on average, roughly exponentially with increasing EA, $P \propto \exp(EA/\varepsilon_A)$, i.e., with a characteristic upslope energy ε_A of only 0.14 eV, red dashed line. However, as indicated by the vertical dash-dotted line, normalized ion fractions for one specific value of EA may differ by more than 2 orders of magnitude. This unsatisfactory order of the experimental data needs to be improved significantly, the prime original aim of this study. As to the high end of EA, we note that $P_{i,F}$ exhibits a constant level for EA > 2.5 eV (data for EA > 3 eV are due to the halogens up to iodine). The reason for this kind of yield saturation is not known presently.

To roughly convert the normalized ion yields of Figure 1 to absolute negative ion fractions, one can make use of a recent evaluation[6] which suggested that about 6% of all Si atoms sputtered from silicon by normally incident 10 keV Cs are emitted as negative ions. Accounting for the decrease in ion fraction with increasing impact energy[15] and angle,[16] the Si^- ion fraction for 14.5 keV at 25° is estimated to be a factor of about 3 to 4 lower, i.e., 1.5−2%. The normalized ion fraction of Si^- in Figure 1 is 0.14 so that the plateau level $P_{i,F} = 1$ roughly corresponds to an absolute ion fraction of 0.10 to 0.14.

Periodicity of Normalized Ion Yields. An interesting aspect of Figure 1 is that, with reference to their position in the periodic table of elements, the yield data are not statistically distributed around some hypothetical mean dependence on EA. Rather, they exhibit a kind of systematic order. For example, the normalized ion fractions of the light elements ^{1}H, ^{5}B, ^{6}C, ^{8}O, and ^{15}P are located to the very left of the data set, the period-5 transition elements ^{41}Nb, ^{42} Mo, ^{44}Ru, and ^{45}Rh appear on the opposite side. To examine this aspect further, all 63 ion yields[5] are compiled in Figure 2 as a function of the atomic number *Z*, distinguished by period (or row). Lanthanides (Lan) and actinides (Act) are marked separately. The data are distributed over the whole periodic table, an admirably complete piece of work.[5] With the exception of the first period p1, which comprises only H and He, all other periods (p2 to p6) exhibit variations in normalized ion yield by up to 6 orders of magnitude. The maximum normalized ion fraction of unity is achieved in all periods (the yield of ^{79}Au in period 6 is slightly lower, 0.7, but 1.0 in the 1991 data, see Figure 1). The lack of a *Z*-dependence in maximum yield suggests that the authors[4,5] were successful in setting up their instrument in such a way that they achieved ion detection independent of secondary ion mass. Hence, at least for the high-yield elements, the assumption $T_r\varsigma_r/T_i\varsigma_i = 1$ appears to be justified.

As the gray dash-dotted lines in Figure 2 indicate, the normalized negative-ion yields also exhibit systematic changes within groups of the periodic table. Remarkable local minima are observed for group-13 elements of periods 4 to 6, i.e., for ^{31}Ga, ^{49}In, and ^{81}Tl.

dx.doi.org/10.1021/ac501006g | Anal. Chem. 2014, 86, 5962−5968

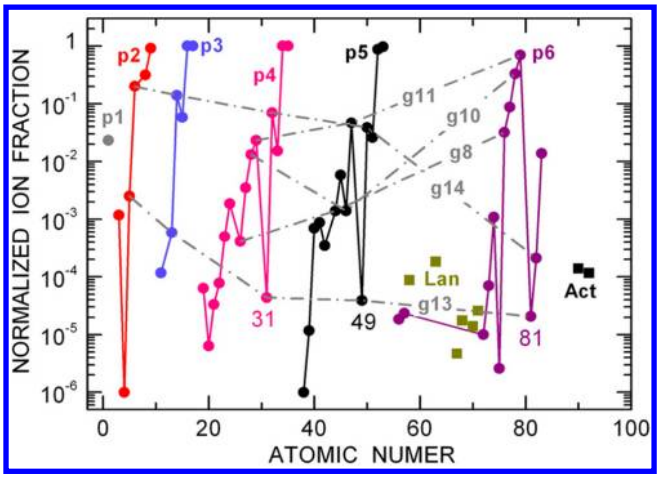

Figure 2. Negative ion fractions of elements (ref 5) versus atomic number, specified by period and group, *p* and *g*, respectively.

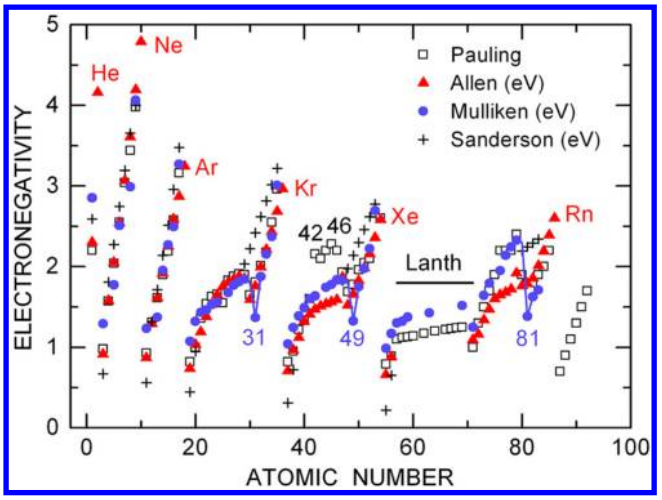

Figure 3. Comparison of the electronegativity of elements derived from different sources (refs 21−26).

RESULTS AND DISCUSSION

Concept of Data Evaluation. The starting point of the following evaluation is the hypothesis that the large scatter of the data in Figure 1 is due to the fact that the electron affinity is not the only element specific property determining the charge state of a sputtered atom. Extending a concept sketched recently,[6] ion formation may formally be considered a two-step process.

The first step involves the breaking of the bond(s) between the ejected atom and its neighbor (or neighbors) at the surface of the ion bombarded sample. As such, the idea of bond breaking is not new.[17−19] Detailed models for positive ion emission from oxides, however, predict ion yields to depend on the emission velocity. In analogy to the case of Cs-enhanced negative ion emission,[6] this concept has no basis, as one can tell from the fact that measurements of oxygen-induced yield enhancement are commonly performed at the low-energy peak of the energy spectrum, without significant spectral changes,[6] except for a possible shift due to changes in work function.[20] Here it is argued that the probability of forming ion scales with the ionic contribution to the bond, quantified by the difference in electronegativity $\Delta\chi_{i,X} = \chi_i - \chi_X$, where X denotes atoms with which the dopant atom i formed a bond prior to sputter ejection. The logic of the reasoning implies that in this case X denotes Cs. Whether the sputtered atom will actually be able to depart as an ion depends on its electron affinity, i.e., on the energy gained by attaching an electron in the formal second step of the ion formation process. We examine the reasonable idea that the normalized ion fractions depend on the sum of $\Delta\chi_{i,Cs}$ and EA_i, i.e.,

$$P_{i,F} = f(\Delta\chi_{i,Cs} + EA_i) \quad (4)$$

Well below the saturation region one may expect an exponential dependence, but independent confirmation is required.

Comparison of Proposed Electronegativity Data. Four sets of electronegativity data are compared in Figure 3, due to concepts of Pauling,[21,22] (for refined data, see CRC Handbook[23]), Mulliken,[24] Sanderson,[25] and Allen[26] (a few individual data not included in the original work were taken from updated tables published in www.wikipedia.org). Whereas the Pauling electronegativity is dimensionless due to normalization,[22] the three other concepts provide data in units of energy (commonly in eV). For internal consistency, the Pauling data are also read in eV throughout this study. This is justified because the original data derived by authors other than Pauling were scaled to achieve the same range of numerical values as Pauling, with arbitrarily selected reference element(s), e.g., F[25] or Ge and As.[26]

In terms of the dependence on atomic number *Z*, the data in Figure 3 exhibit similarities in that the electronegativity mostly increases monotonically within each period of the periodic table. However, there are quite a few pronounced differences in detail. The χ values derived by Sanderson deviate sometimes strongly from the three other sets of results and, very important with reference to the aim of this study, the number of data is only $N = 39$. Hence, Sanderson's data could not be included in the evaluation presented below. As to the other three sets of data, two remarkable local differences in the *Z*-dependence of χ deserve attention. First, in the range $42 \le Z \le 46$, χ(Pauling) exceeds the common trend abruptly by between ca. 0.5 eV (compared to Mulliken) and 0.7 eV (Allen). Second, χ(Mulliken) exhibits pronounced minima for the "poor" metals ^{31}Ga, ^{49}In and ^{81}Tl, in analogy to the minima in Figure 2 at the same *Z*. Interestingly, the minima are present in much reduced form in χ(Pauling) and they are essentially absent in χ(Allen).

Mulliken[24] presented arguments that the *absolute* electronegativity is simply the arithmetic mean of the electron affinity and the ionization potential. The derived *relative* electronegativity χ_{Mull} is commonly written

$$\chi_{Mull} = \chi_0 + \beta(EA + IP) \quad (5)$$

with $\chi_0 = 0.17$ eV and $\beta = 0.187$.[27] The scaling parameters in eq 5 are debatable. A fit to Pauling's data of similar, if not better, quality is obtained setting $\chi_0 = 0$ and $\beta = 0.204$. The ratio χ_{Mull}/χ_{Pau} is 1.02 ± 0.17 in the former case and 1.00 ± 0.15 in the latter.

According to the Mulliken concept, eq 5, the electronegativity is predicted to increase linearly with increasing electron affinity and ionization potential. In Figure 4, the very close correlation of the electronegativity with the ionization potential is evident. The constant (zero offset) derived by linear regression analysis (straight lines in Figure 4) is less than ±0.1 eV, and the *R* values exceed 0.90 in all three cases of interest, i.e., Pauling, Allen, and Mulliken. Hence, if eq 5 applies, we are led to the rather exciting conclusion that the probability for an

dx.doi.org/10.1021/ac501006g | Anal. Chem. 2014, 86, 5962−5968

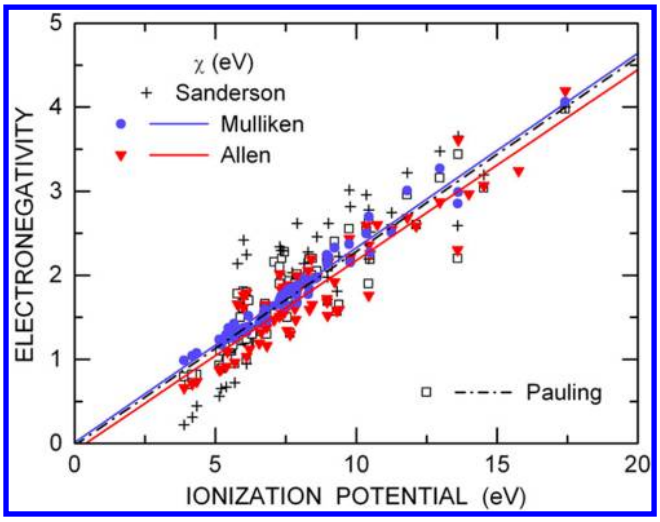

Figure 4. Electronegativity data of Figure 3 versus the ionization potential.

atom to being sputtered as a negatively charged ion should depend not only on its electron affinity but also on its ionization potential. In support of this statement, Figure 5

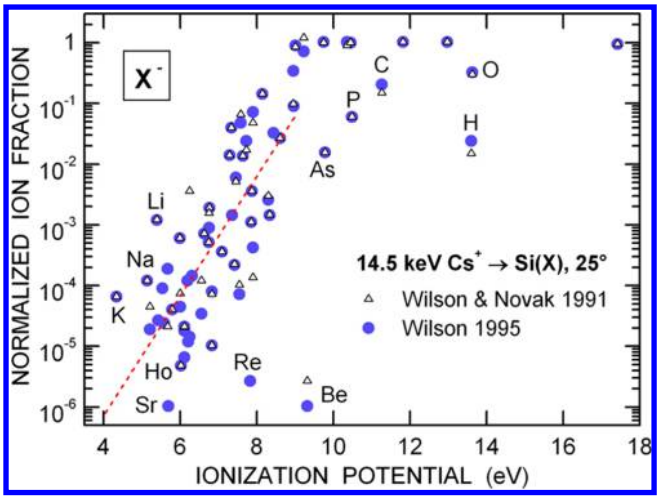

Figure 5. Negative ion fractions versus the ionization potential.

shows all ion fractions derived from the work of Wilson and Novak[5] and Wilson[6] as a function of the ionization potential. Note that the negative ion fractions *increase* with increasing IP, just opposite to the case of positive secondary ion emission. The mean rise may again be represented by an exponential dependence (red dashed line), $P \propto \exp(\mathrm{IP}/\varepsilon_I)$, with a characteristic energy ε_I = 0.44 eV. Eight experimental data that could not be included in Figure 1 because of missing information on the electron affinity are now present in Figure 5, e.g., Be, Ho, and Re. A comparison of Figures 1 and 5 reveals many gross similarities, but the order of the data is often inverted: elements observed to the very left in Figure 1 (such as H, C, O, and P) appear on the opposite side in Figure 5.

To complete assessment of the correlation between electronegativity and atomic properties, the dependence on electron affinity, Figure 6, is seen to be much more complex than in Figure 4. At a fixed value of EA, the χ values can differ strongly. This is largely due to the dominant contribution of IP to χ. One may, however, consider the strong variation of χ in Figure 6

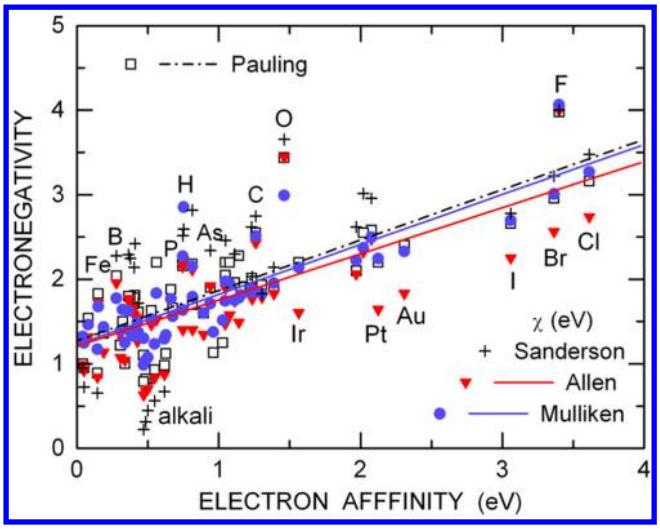

Figure 6. Electronegativity data of Figure 3 versus the electron affinity.

desirable because it could mean that the sum χ + EA is the parameter providing improved order of the normalized ion fractions.

Validating the Proposed Concept of Ion Formation. Convincing evidence in support of the idea that the sum χ + EA is the appropriate parameter for organizing negative ion yields is presented in Figure 7. The orange down-triangles are shown

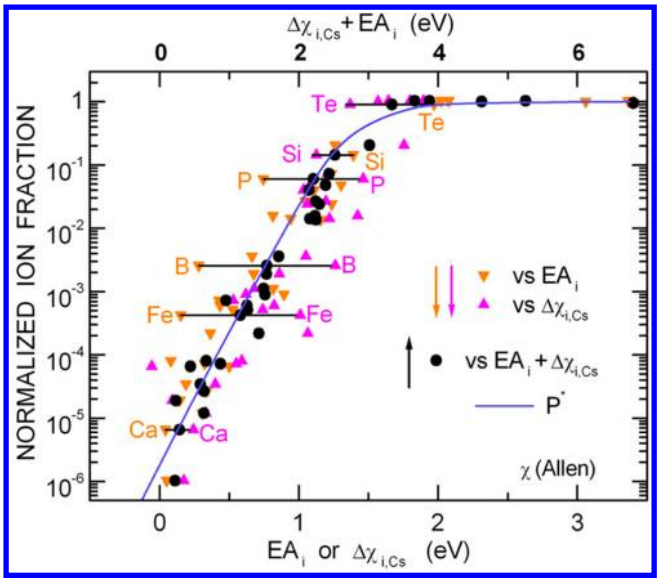

Figure 7. Selected negative ion fractions versus three different variables: (i) the electron affinity, (ii) the electronegativity of Allen (bottom scale), and (iii) versus the sum of the two variables (top scale). For details, see text.

in the same way as in Figure 1, i.e., as a function of EA_i. For clarity only a limited number of 36 data is included, selected by the criterion that the difference between the χ values of Pauling, Allen, and Mulliken, $|\delta\chi_{PAM}|$, should be less than 0.34 eV. This way the whole range of normalized ion fractions, from 10^{-6} to 1, is covered (total number of selected χ-data N = 38; no ion yields available for Rb and Cs). The magenta up-triangles represent the same data as the orange down-triangles but are plotted as a function of $\Delta\chi_{i,Cs}$, with χ values of Allen. Here and in the detailed evaluation presented below the same reference

dx.doi.org/10.1021/ac501006g | Anal. Chem. 2014, 86, 5962−5968

electronegativity χ_{Cs}(Pauling) = 0.79 eV was used because it is close to the mean of the two other alternative choices, 0.66 eV (Allen) and 0.99 eV (Mulliken). In doing so, one avoids an arbitrary shift between the three sets of $\Delta\chi_{i,Cs}$-data.

The exciting aspect of Figure 7 is that the "outliers" observed on the scale of EA_i appear, in many cases, almost exactly on the opposite side of the same data set when shown as a function of $\Delta\chi_{i,Cs}$. This is very much in analogy to the "inverted" location of the data in Figures 1and 5. Extreme examples of outliers in Figure 7 are P, B, Fe, and K. However, plotting the ion fractions a third time (black solid circles), now as a function of $\Delta\chi_{i,Cs}$ + EA_i, (top scale), the data exhibit a common trend, i.e., they scatter quite closely around an assumed "master" curve P^* (blue line; details concerning the analytical form of P^* are discussed below).

Including all ion fractions with known electron affinity, Figure 8 shows a compilation of data versus $\Delta\chi_{i,Cs}$ + EA_i, for all

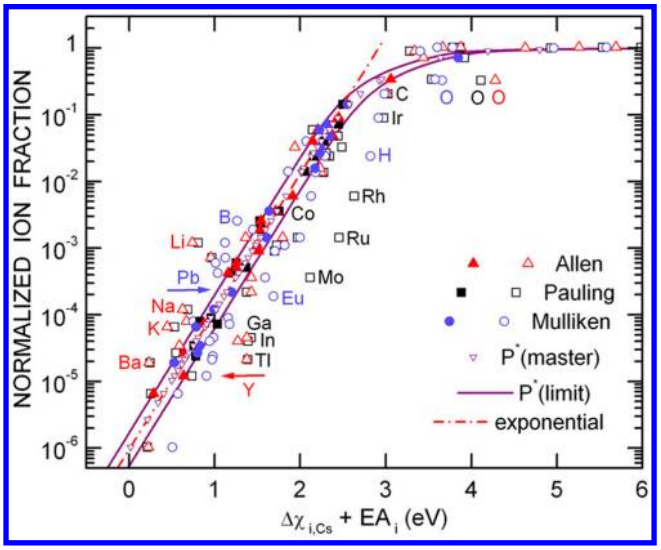

Figure 8. Negative ion fractions versus the sum of electron affinity and electronegativity, for three alternative choices of the electronegativity. The lines define the assumed region of validity of selected subsets of the electronegativity data (solid symbols). For details, see text.

three choices of χ (open symbols) [N = 54 (Pauling), 52 (Allen), and 55 (Mulliken)]. Evidently, the majority of the data (N = 35), full symbols, is located within the narrow "region of validity" between the two purple lines, denoted P^*(limit). The two lines are separated from the mean, P^*(master), purple down-triangles, by only ±0.12 eV. Taking into account that seven elements of groups 16 and 17 with $P_{i,F} \cong 1$ (see Figure 2) are meaningless for this kind of test, we find that 76% of the useful data (35 out of 46) comply with the chosen criterion of validity. For $P_{i,F} < 0.2$, the valid data (33/46) can be well described by an exponential dependence,

$$P_{i,F} = P_0 \exp[(\Delta\chi_{i,Cs} + EA_i)/\varepsilon_{\chi,A}] \quad (6)$$

with $P_0 = 9.5 \times 10^{-7}$ and $\varepsilon_{\chi,A}$ = 0.21 eV.

Taking a closer look at the data, several observations are noteworthy. In many cases only one out of three χ values available for a certain element fits well into the region of validity. Two examples are highlighted by horizontal arrows, ^{82}Pb (blue, fit-only Mulliken) and ^{39}Y (red, fit-only Allen). Out of the 35 "valid cases", 16 are from χ(Pauling), 18 from χ(Allen), and 16 from χ(Mulliken), with 21 singles, 13 duplicates, and 1 triplicate (^{27}Co). The number of valid cases could be enlarged, mostly in favor of Pauling and Mulliken, by slightly extending the width of the validity interval to ±0.15 eV, for example. But this would not have an effect on P^*(master). In essence, all three sources of electronegativity are equivalent for the present purpose, but each of them provides only a partial contribution. The data in Figure 8 also serve to document the fact, partly addressed already in the discussion of Figure 3, that the χ values from different sources sometimes exhibit extremely large and often systematic deviations from the mean trend.

Deriving Refined Electronegativity Data. The results of Figure 8 suggest that it is not meaningful to examine available electronegativity data with the aim of identifying the "most appropriate" compilation. Instead the selected data merely serve as the backbone for determining P^*(master) which is considered to represent the ideal situation in which case the "correct" electronegativity χ_{SIMS} to be assigned to the respective element would already be known beforehand (open down-triangles). Turning arguments around, we now set out to determine $\chi_{i,SIMS}$. For this purpose, we need to determine the analytical function that assigns an element with an ion fraction $P_{i,F}$ its position $\Delta\chi_{i,Cs}$ + EA_i according to P^*(master) . Hence, instead of $y(x)$ the inverse function $x(y)$ is required. In the region where eq 6 applies, this is a simple task, i.e., $x(y) \propto \ln P_{i,F}$. Two additional terms were added to simulate the transition from an exponential rise to saturation,

$$[\Delta\chi_{i,F} + EA_i] = \varepsilon_0 \ln\left(\frac{P_{i,F}}{P_0}\right) + a_1 P_{i,F}^r + a_2 P_{i,F}^s \quad (7)$$

The factors a_1 and a_2 as well as the exponents r and s must be optimized by "good guess". Fortunately, the chosen numbers (a_1 = 1.3 eV, a_2 = 2.7 eV, r = 1.5, and s = 25) affect $\chi_{i,SIMS}$ only for three elements, ^{8}O, ^{78}Pt, and ^{79}Au. The two blue lines defining the region of validity in Figure 8 were also derived from eq 7 but with ±0.12 eV added on the right-hand side. Knowing the sum $[|\Delta\chi_{i,F} + EA_i|]$ for each element, $\chi_{i,SIMS}$ is simply

$$\chi_{i,SIMS} \equiv \Delta\chi_{i,Cs} + \chi_{Cs} = [\Delta\chi_{i,F} + EA_i] - EA_i + \chi_{Cs} \quad (8)$$

Note again that once a decision has been made concerning the shape of P^*, $\chi_{i,SIMS}$ is solely determined by the experimentally determined ion fraction $P_{i,F}$.

Results for $\chi_{i,SIMS}$ (or briefly χ_{SIMS}) are compiled in Figure 9a as solid diamonds. The total number of elements for which the SIMS-based electronegativity could be determined is 48. The seven elements of groups 16 and 17 with $P_{i,F} \cong 1$ could not be evaluated because very slight variations of $P_{i,F}$ in the vicinity of 1 give rise to large variations of $[\Delta\chi_{i,F} + EA_i]$, so that χ_{SIMS} is ill defined. To document the correlation with the χ values of Pauling, Allen, and Mulliken, the favorable data are superimposed on χ_{SIMS} in Figure 9b (not all data visible due to occasional overlap).

Trying to correlate χ_{SIMS} with previous concepts of electronegativity, only the model of Mulliken allows variations in absolute number because χ_0 and β in eq 5 may be treated as adjustable parameters. It turned out that χ_{SIMS} can modeled quite well even with a simplified version of eq 5, setting χ_0 = 0 and removing the dependence on EA, so that the calculated electronegativity is solely dependent on the ionization potential, $\chi_{IP} = \beta$IP, in accordance with Figure 4. An advantage

dx.doi.org/10.1021/ac501006g | Anal. Chem. 2014, 86, 5962−5968

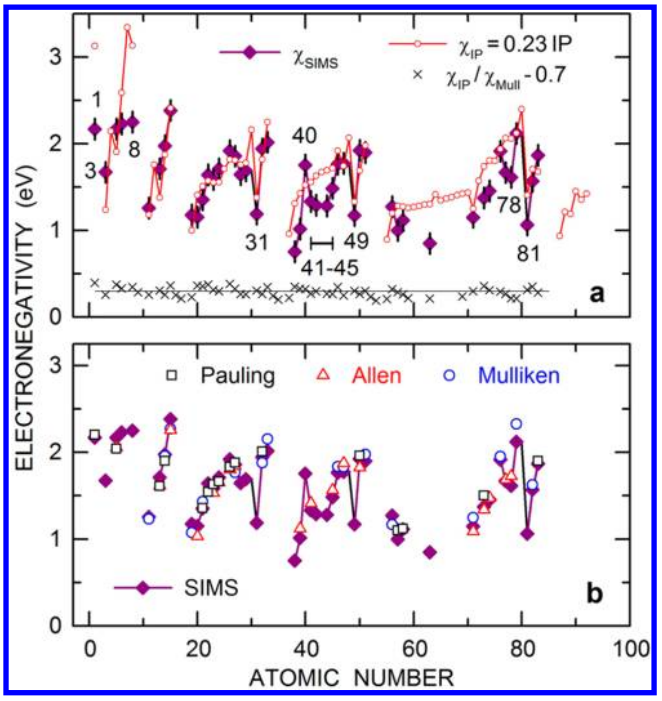

Figure 9. (a) SIMS-based electronegativity versus atomic number, compared with predictions due to a simplified Mulliken model involving only a dependence on ionization potential. The ratio to the standard Mulliken model is shown as crosses. (b) Comparison of the SIMS-based electronegativity with selected data due to Pauling, Allen, and Mulliken.

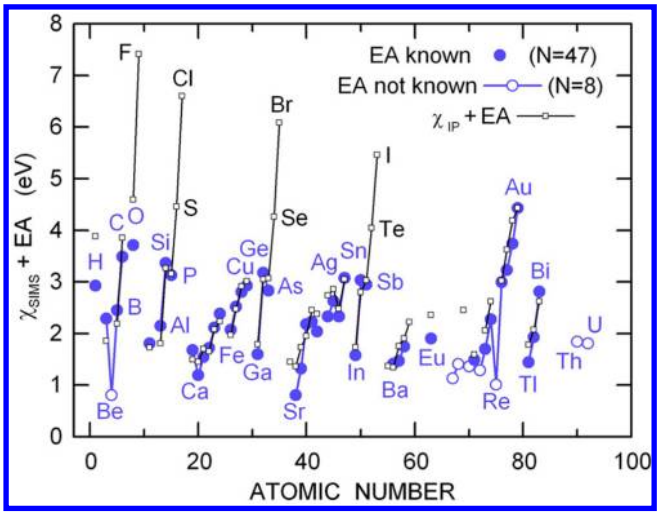

Figure 10. Sum of electronegativity and electron affinity versus atomic number. SIMS-based data are compared with Mulliken-type predictions.

is that χ_{IP} can be determined for all elements; knowledge of EA is not required. The factor β determines the agreement between χ_{SIMS} and χ_{IP} in terms of their gross Z-dependence. Results for β = 0.23 are depicted in Figure 9a as open red circles. Comparison of χ_{IP} with the standard χ_{Mull} shows that the difference is small, as one can tell from the ratio χ_{IP}/χ_{Mull} = 0.99 ± 0.05. The Z-dependence of the (dimensionless) ratio, shifted downward by 0.7 for clarity, is shown by the crosses near the bottom of Figure 9a. The small difference illustrates (again) that a Mulliken-based determination of the electronegativity is not very sensitive to (reasonably small) variations of the factors assigned to the contributions due to EA and IP.

To add to the overall good agreement between χ_{SIMS} and χ_{IP}, we note that the repeatedly mentioned sharp minima observed at Z = 31, 49, and 81 are very similar in the two sets of data. The agreement provides confidence that the approach used to determine χ_{SIMS} has a solid basis. The minima in the χ_{SIMS} data reflect the fact that the ion fractions of Ga, In, and Tl exhibit deep minima on the Z-scale; see Figure 2. The outer-shell configuration of these elements is $(n-1)d^{10}ns^2np^1$, with n = 4, 5, and 6. The supposition is that the p^1 electron is the cause of the minima. Recall that, whereas the minima are well established in χ_{Mull} or χ_{IP}, they are not evident in the data of Allen and poorly defined or displaced (Z = 30 and 48) in Pauling's compilation; see Figure 3. The origin of the difference deserves attention.

Addressing differences between χ_{SIMS} and χ_{IP} in Figure 9a, the largest effects are seen for the light elements ^{1}H, ^{3}Li, and ^{8}O. Rather irritating is the finding that $\chi_{SIMS} < \chi_{IP}$ for H and O, but $\chi_{SIMS} > \chi_{IP}$ for Li. In the case of oxygen, a likely reason for the difference is the strong reaction of this element with cesium.[6] Hence, a sizable fraction of the implanted oxygen may be sputtered as Cs_nO_m molecules, neutral or ionized, but lost for O^- production. According to Figure 8, an upward correction of the O^- yield by a factor of 2 would suffice to produce reasonable agreement between χ_{SIMS} and χ_{IP}. In support of this argument, Figure 10 shows that the predicted sum χ_{IP} + EA is even higher for O than for S. Yet $P(S^-)$ is 1.0. Without the conceivable artifacts, $P(O^-)$ should thus also be (close to) unity.

Significant local differences between χ_{SIMS} and χ_{IP} are also evident for certain transition elements of period 5 and 6. More specifically, the χ_{SIMS} values for ^{41}Nb, ^{42}Mo, ^{44}Ru, ^{45}Rh, and ^{78}Pt exhibit distinct negative deviations from the common trend represented by χ_{IP}. Interestingly, the outer-shell electron configuration of theses elements is $(n-1)d^{g-1}ns^1$. Much like the presumably p^1-related minima discussed above, the s^1 electron could be the cause of the lower-than-normal electronegativity. If these findings could be substantiated by future work, they would document a remarkable power of secondary ion mass spectrometry to provide chemical information not accessible by other analytical techniques.

Further to Figure 10, the data are primarily meant to show the intimate correlation with the data in Figure 2. If the three elements O, Pt, and Au located in the region $0.2 < P_{i,F} < 1$ are ignored, $[\Delta\chi_{i,F} + EA_i]$ equals log $P_{i,F}$, except for a calibration factor. The results suggest that ion yields will saturate as soon as $[\Delta\chi_{i,F} + EA_i]$ exceeds about 4.5 eV. Another purpose of Figure 10 is to draw attention to the fact that $[\Delta\chi_{i,F} + EA_i]$ can be derived from ion yields even if EA_i is not known. Examples are the elements represented by open circles.

A few remarks are in order concerning accuracy of the SIMS data basis. In the discussion of Figure 1 it was already mentioned that the compilations of 1991 and 1995 occasionally exhibit significant if not pronounced differences of unknown origin. The reported RSF values[4,5] may be affected by many sources of error which cannot be discussed in any detail here except for noting that the ion yield ratios must be expected to vary with the choice of the apertures used in the secondary ion beamline, as discussed in two closely related recent studies.[28,29]

Another aspect of concern is the lack of experimental electron affinity data for a variety of elements, notably the

dx.doi.org/10.1021/ac501006g | Anal. Chem. 2014, 86, 5962−5968

lanthanides. In cases where such data were reported, based on laser photodetachment electron spectroscopy,[11,12] they were sometimes completely at variance with theoretical data, like those obtained by relativistic configuration−interaction calculations.[30] Two extreme examples may suffice. (1) ^{63}Eu: experiment EA = 1.053 ± 0.025 eV,[12] calculation 0.117 eV;[30] (2) ^{69}Tm: 1.029 ± 0.022 eV[11] vs 0.022 eV.[30] It has been noted[30] that the photodetachment data are "contradicting earlier accelerator mass spectrometry studies".[31] The discrepancies between results obtained by different experimental techniques need to be resolved. It is worth mentioning that the abundance of negative ion beams generated in Cs-based ion sources of tandem accelerator has been interpreted on the basis of the tunneling model.[31] As described here and elsewhere,[6] such an approach is misleading.

CONCLUSION

This study has shown, for the first time, that it is possible to correlate measured ion yields, varying by more than 6 orders of magnitude, in a quantitative manner with atomic properties of the sputtered atom. Evidently, the ability to produce a negative secondary ion does not only depend on the electron affinity, as assumed previously, but also on the ionic contribution to the bond between the sputtered atom and the yield enhancing species, in this case cesium (note that we are dealing here with an elemental target, not an ionic compound). The ionic contribution to the local bond can be quantified by the electronegativity which means that, surprisingly, negative ion yields are intimately correlated with the ionization potential of the sputtered atom.

A straightforward test of the new model was significantly aggravated by the fact that established electronegativity tables exhibit sometimes pronounced differences. Nevertheless selected subsets of the compilations served well to establish a backbone for deriving refined, so-called SIMS-based electronegativity data which, overall, are in support of the theoretical concept of Mulliken. To the author's knowledge, this is the first example of an experimental technique that allows a multielement comparison of the electronegativity. The evaluation presented above was limited to results for a host matrix of silicon, the reason being that there is no other set of data comprising as many as the 63 dopant elements available here. Less complete RSF compilations have been reported for a variety of other matrixes.[1] Such data should be well suited to test the general validity of the new model. However, to identify and possibly quantify the effect of matrix dependent differences in the availability of Cs at the surface, it would be desirable to have access to absolute ion yields rather than just RSF data.

Future work should address the very details of ion formation. Possible pitfalls, such as yield losses due to excessive reaction with cesium, also need to be explored.

AUTHOR INFORMATION

Corresponding Author

*Fax: +49-89-3187-3323. E-mail: wittmaack@helmholtz-muenchen.de.

Notes

The authors declare no competing financial interest.

ACKNOWLEDGMENTS

The scientific progress achieved in this study rested on the availability of a remarkably extended set of secondary-ion yield data assembled by Bob Wilson and his co-workers in very elaborate work lasting many years. In the past, the importance of their data has been strongly underestimated by the scientific community. We should thank Bob Wilson and his group for their contribution.

REFERENCES

(1) Novak, S. W.; Wilson, R. G. *J. Appl. Phys.* **1991**, *69*, 463−465.
(2) Stevie, F. A.; Wilson, R. G. *J. Vac. Sci. Technol., A* **1991**, *9*, 3064−3070.
(3) Stevie, F. A.; Kahora, P. M.; Cochran, G. W. *J. Vac. Sci. Technol., A* **1991**, *9*, 1385−1389.
(4) Wilson, R. G.; Novak, S. W. *J. Appl. Phys.* **1991**, *69*, 466−474.
(5) Wilson, R. G. *Int. J. Mass Spectrom.* **1995**, *143*, 43−49.
(6) Wittmaack, K. *Surf. Sci. Rep.* **2013**, *68*, 108−230.
(7) Wittmaack, K. In *Secondary Ion Mass Spectrometry SIMS XI*; Gillen, G.; Lareau, R.; Bennett, J.; Stevie, F., Eds.; Wiley: Chichester, UK, 1998; pp 11−18.
(8) Deline, V. R.; Katz, W.; Evans, C. A., Jr.; Williams, P. *Appl. Phys. Lett.* **1978**, *33*, 832−835.
(9) Rienstra-Kiracofe, J. C.; Tschumper, G. S.; Schaefer, H. F., III; Nandi, S.; Ellison, G. B. *Chem. Rev.* **2002**, *102*, 231−282.
(10) Davis, V. T.; Thompson, J. S. *J. Phys. B: At., Mol.Opt. Phys.* **2001**, *34*, L433−L437.
(11) Davis, V. T.; Thompson, J. S. *Phys. Rev. A* **2002**, *65*, 010501.
(12) Davis, V. T.; Thompson, J. S. *J. Phys. B: At., Mol.Opt. Phys.* **2004**, *37*, 1961−1965.
(13) Walter, C. W.; Gibson, N. D.; Li, Y.-G.; Matyas, D. J.; Alton, R. M.; Lou, S. E.; Field, R. L., III; Hanstorp, D.; Pan, L.; Beck, D. R. *Phys. Rev. A* **2011**, *84*, 032514.
(14) Knoll, L.; Bhushan, K. G.; Altstein, N.; Zajfman, D.; Heber, O.; Rappaport, M. L. *Phys. Rev. A* **1999**, *60*, 1710−1712.
(15) Wittmaack, K. *Surf. Sci.* **1983**, *126*, 573−580.
(16) Wittmaack, K. *J. Vac. Sci. Technol., A* **1985**, *3*, 1350−1354.
(17) Slodzian, G. *Surf. Sci.* **1975**, *48*, 161−186.
(18) Williams, P. *Surf. Sci.* **1979**, *90*, 588−634.
(19) Yu, M. L. *Nucl. Instrum. Methods B* **1987**, *18*, 542−548.
(20) Blaise, G.; Slodzian, G. *Surf. Sci.* **1973**, *40*, 708−714.
(21) Pauling, L. *J. Am. Chem. Soc.* **1932**, *54*, 3570−3582.
(22) Pauling, L. *The Nature of the Chemical Bond*; Cornell University Press: Ithaca, NY, 1960.
(23) Lide, D. R. *CRC Handbook of Chemistry and Physics*, 86th ed.; Taylor and Francis: Boca Raton, 2005−2006.
(24) Mulliken, R. S. *J. Chem. Phys.* **1934**, *2*, 782−793; **1935**, *3*, 573−585.
(25) Sanderson, R. T. *J. Am. Chem. Soc.* **1983**, *105*, 2259−2261.
(26) Allen, L. C. *J. Am. Chem. Soc.* **1989**, *111*, 9003−9011.
(27) Huheey, J. E. *Inorganic Chemistry*, 2nd ed.; Harper & Row: New York, 1978.
(28) Wittmaack, K. *Int. J. Mass Spectrom.* **2014**, *359*, 55−63.
(29) Wittmaack, K.; Gnaser, H. *Int. J. Mass Spectrom.* **2014**, *358*, 49−58.
(30) O'Malley, S. M.; Beck, D. R. *Phys. Rev. A* **2008**, *78*, 012510.
(31) Nadeau, M. J.; Garwan, M. A.; Zhao, X. L.; Litherland, A. E. *Nucl. Instrum. Methods B* **1997**, *123*, 521−526.